Appl. Phys. B 75, 803–815 (2002)
DOI: 10.1007/s00340-002-1049-7

Applied Physics B
Lasers and Optics

F. BONNEAU[1,✉]
P. COMBIS[1]
J.L. RULLIER[1]
J. VIERNE[1]
M. PELLIN[2]
M. SAVINA[2]
M. BROYER[3]
E. COTTANCIN[3]
J. TUAILLON[3]
M. PELLARIN[3]
L. GALLAIS[4]
J.Y. NATOLI[4]
M. PERRA[4]
H. BERCEGOL[5]
L. LAMAIGNÈRE[5]
M. LOISEAU[5]
J.T. DONOHUE[6]

Study of UV laser interaction with gold nanoparticles embedded in silica

[1] Département de Physique Théorique et Appliquée, CEA/DAM Ile de France, BP 12, 91680 Bruyères le Châtel, France
[2] Materials Science Division, Argonne National Laboratory, Argonne, IL 60439, USA
[3] Centre Agrégat LASIM and DPM, Université Claude Bernard Lyon 1 and CNRS, 69622 Villeurbanne, France
[4] Institut Fresnel, Domaine Universitaire de St. Jérôme, 13397 Marseille, France
[5] Département des Lasers de Puissance, CEA/Centre d'Etudes Scientifiques et Techniques d'Aquitaine, BP 2, 33114 Le Barp, France
[6] Centre d'Etudes Nucléaires de Bordeaux-Gradignan, BP 120, 33175 Gradignan, France

Received: 19 July 2002/Revised version: 23 September 2002
Published online: 11 December 2002 •

ABSTRACT In order to resolve problems concerning the understanding and the control of laser-induced damage of silica optical elements, a collaboration between the CEA and different university laboratories has been undertaken. Ultra-pure silica model samples, seeded with gold nanoparticles whose diameter did not exceed 5 nm, were prepared. The aim in using these samples was to observe the mechanism of damage initiation that could be attributed to inclusions of nanometric size. This paper presents the different steps encountered during this study: preparation of the samples, the laser-induced damage tests, the Nomarski and atomic-force microscope observations of this damage and a series of experiments using a time-of-flight mass spectrometer at Argonne National Laboratory. The experimental data are then interpreted, and, in particular, compared to numerical simulations. A very encouraging result is the existence of a pre-damage phase at very low fluences that is not detectable by classical optical devices. The experimental means developed for such model samples should be transposable to the analysis of industrial glasses.

PACS 61.80.Ba; 42.70.-a; 52.38.Mf

1 Introduction

The construction both in France and in the USA of large lasers designed to study nuclear fusion via inertial confinement represents one of the major technological challenges of the next decade. One of the most important problems met in the operation of these lasers at the National Ignition Facility (NIF) at Lawrence Livermore National Laboratory (LLNL) and the Laser Mégajoule (LMJ) at Commissariat à l'Energie Atomique (CEA), concerns the fragility of optical glass subjected to the high flux [1, 2]. Indeed, the extremely high fluxes lead to many optical components of the laser chain being subjected to fluences greater than 20 J/cm^2 at the fundamental frequency ($\lambda = 1.053\ \mu$m) or 10 J/cm^2 at the tripled frequency ($\lambda = 0.351\ \mu$m).

The appearance of surface damage on optical components is caused mainly by the presence of residual defects of sub-micron size in the glass, such as microscopic fractures stemming from polishing, bubbles and metal or dielectric inclusions [3–7]. These defects absorb energy from the laser, and serve as nuclei for damage, which appears at interfaces in the form of craters following the laser pulse. Investigations of such laser-induced damage have been carried out for many years [8–10], and have led to improvements in glass quality and polishing, which have resulted in higher damage resistance. However, a more detailed understanding of the damage process requires an analysis of precursor phenomena, which are not detectable by the usual optical methods. In damage studies, industrial glass poses a problem in that the size, the chemical composition and the location of the various defects it contains are generally unknown. The only data we have concerns the concentration of certain metals (in particular, aluminum) present at the trace level [11]. In order to reduce this uncertainty and to produce reproducible material for tests, following the lead of researchers at the University of Rochester [12] and LLNL [13], we have made model samples containing calibrated gold inclusions encapsulated in ultra-pure silica deposited by evaporation. In these samples, the gold inclusions have diameters of about 3 nm, and are covered by a layer of silica of thickness 130 nm. In preparing the samples we avoided the use of colloids which contain surfactants designed to prevent the inclusions from coalescing into clusters. The residues of these surfactants could pollute the gold particles and make the interpretation of the experimental results more difficult.

With the aim of observing the initiation of damage, we carried out a series of in situ laser damage tests on a time-of-flight mass spectrometer at Argonne National Laboratory (ANL).

✉ Fax: +33-1/6926-7106, E-mail: florian.bonneau@cea.fr

This installation is of great interest because it enables us to combine the laser irradiation of the sample with the chemical identification of material ejected from the sample. An evaluation of the quantity of gold atoms emitted during irradiation can thus be obtained from the experimental results.

The order of this paper is as follows: Sect. 2 contains a description of the sample preparation. Section 3 describes the laser-induced damage tests and methods of observing damage. The time-of-flight mass spectrometer is presented in Sect. 4, and the spectra we found are given in Sect. 5. The results of operating the spectrometer on a shot-by-shot basis over a limited range of masses are discussed in Sect. 6. We discuss the modeling and simulation of the experimental results in Sect. 7 and give our conclusion in Sect. 8.

2 Preparation of the samples

It is, today, a well-known fact that defects of nanometric size can cause damage of micrometric size in tests of resistance to laser fluxes [14, 15]. In order to avoid collective effects among nanoparticles, which would be hard to interpret, it is desirable to obtain a low-density deposit of gold nanoparticles. Our samples were prepared at the Laboratoire de Spectroscopie Ionique et Moléculaire (LASIM) at the Université de Lyon, which has a long experience in the field of clusters and thin films [16, 17]. In particular, the use of a mechanical chopper to reduce the number of gold nanoparticles reaching the sample was a key feature of the preparation. Another essential aspect was to ensure that all the nanoparticles were covered by the same thickness of silica. Here, this was achieved by modifying the standard procedure for bulk deposits. By sequential deposition, first of silica (by bombarding bulk silica with an electron beam), then gold (by evaporating a gold bar with a laser beam), and finally silica, a sandwich-like structure was obtained. A section of such a sample is shown (schematically) in Fig. 1. There one sees the two 130-nm-thick layers of silica deposited on a polished substrate, with gold nanoparticles between the layers. Under these conditions of evaporation, the density of the silica deposited was reduced by approximately 30% compared to glass, which corresponds to porosity in the silica film. Rutherford back-scattering on the silica deposits indicated that the stoichiometry of our samples was SiO_x, with $x = 2.00 \pm 0.05$.

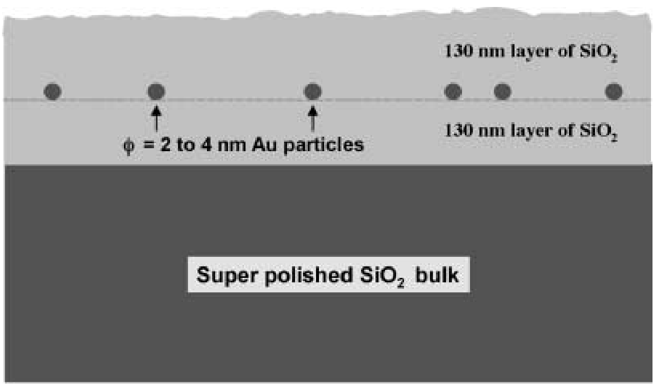

FIGURE 1 Figurative drawing of a section of a sample

We prepared samples with two different densities of nanoparticles, approximately 10 and 100 particles per squared micrometer, which we denote as d_{10} and d_{100}, respectively. Their size was $10\,\mathrm{mm} \times 11\,\mathrm{mm}$. To characterize the surface roughness of the samples we used an atomic force microscope (AFM) [18]. A typical AFM image is shown in Fig. 2, where a $15\,\mu\mathrm{m} \times 15\,\mu\mathrm{m}$ surface has been scanned. The lower part of the figure shows the profile along the horizontal line indicated in the upper part. We deduce that the mean surface roughness is 5 nm, with maximum contrast of about 15 nm. Given this, it is impossible to observe the density of inclusions, since

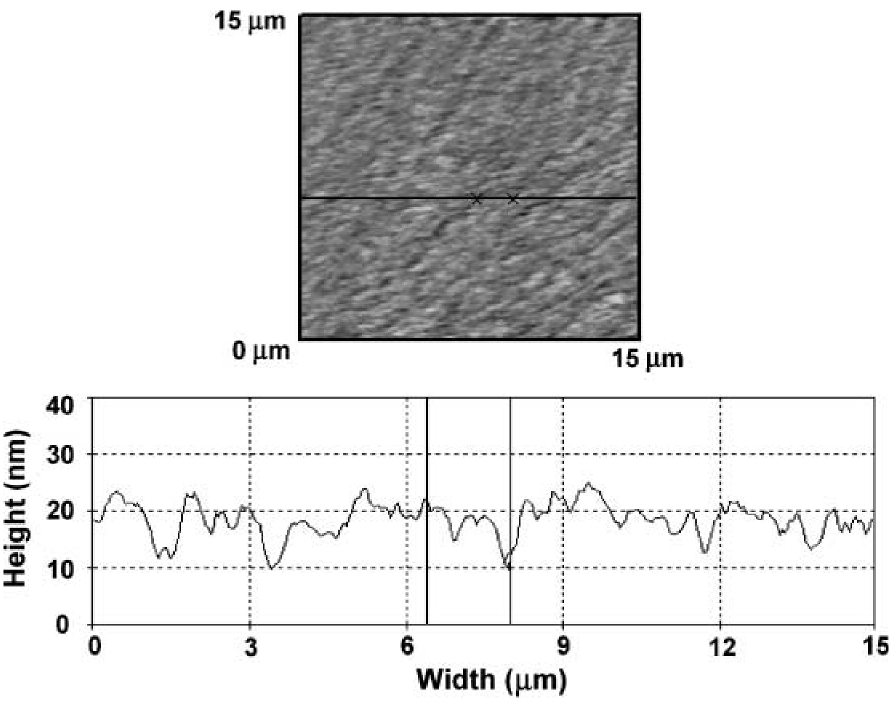

FIGURE 2 AFM image of a sample showing surface rugosity (*upper*). Details of a cut along the *horizontal line*, which furnishes an estimation of the mean surface rugosity (*lower*)

their size of about 3 nm is less than the variation in surface thickness.

3 Sample damage tests

Sample damage experiments were performed at the CESTA damage test facility using a frequency-tripled Nd:YAG laser operating at wavelength 355 nm. The $1/e^2$ beam diameter was 750 µm, and the pulse duration FWHM was 3 ns [19]. Each sample was tested following the procedure called "one-on-one", with one laser shot on each site. The sample was placed with the thin silica layers upstream (i.e. towards the incoming laser beam). The one-on-one damage threshold was then determined by exposing the samples (either d_{10} or d_{100}) to increasing laser fluences while displacing them between shots. All tests were made at normal incidence. Damage was assessed by inspection of the sites with a Nomarski microscope.

For samples containing gold clusters, it has been observed [12] that the nanoparticles are heated and finally vaporized by the absorption of laser light at fluences substantially inferior to those needed to damage highly polished silica. Figure 3 shows, for d_{10} (left) and d_{100} (right) the state of the surface after one shot at a fluence of 4.2 J/cm^2. For the sample of higher density (d_{100}), the silica has undergone heating and fragmentation and has been ejected by the explosion of the inclusions. With the tenfold-reduced density, in contrast, only the first stage of scaling of the surface is observed. Our measurements show that the threshold for the d_{10} sample is 4 J/cm^2, while for d_{100} it is 3 J/cm^2. These results indicate that the damage threshold decreases with inclusion density, as expected.

Additional information was provided by an AFM analysis of a severely damaged site on the d_{100} sample, at a fluence of 4.2 J/cm^2. In the upper part of Fig. 4, the two-dimensional scan suggests that both layers of silica have been removed at

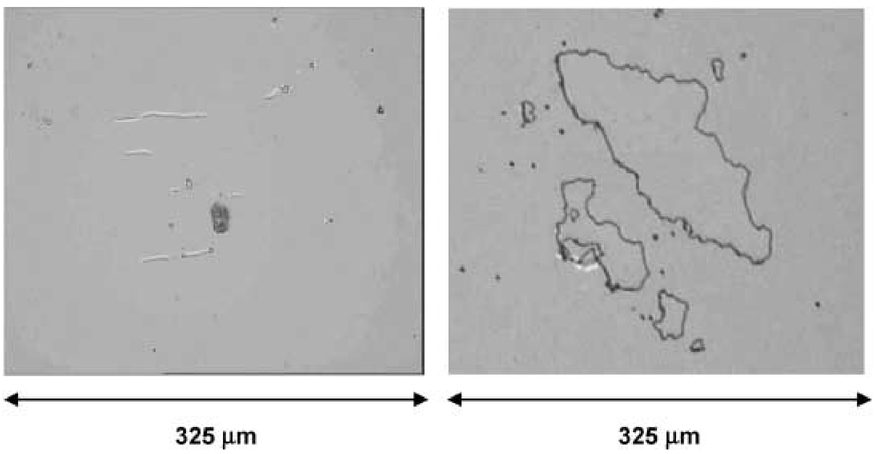

FIGURE 3 Nomarski microscope images of site damage produced at a laser fluence of 4.2 J/cm^2 for samples containing gold nanoparticles: (*left*) density of 10 nanoparticles/µm^2, (*right*) density of 100 nanoparticles/µm^2

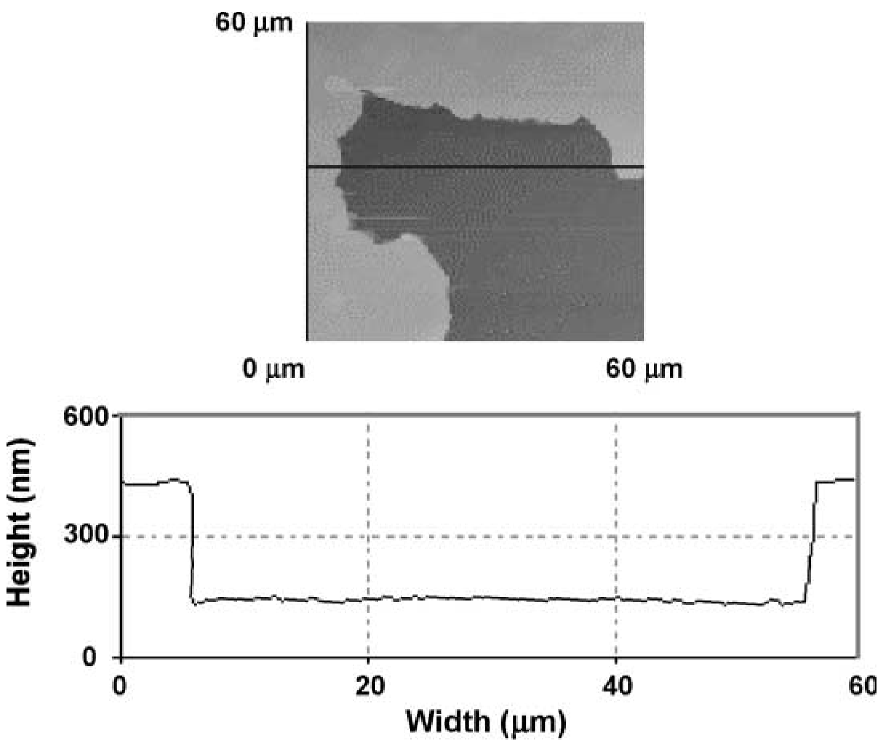

FIGURE 4 AFM observation of a severely damaged site produced at a laser fluence of 4.2 J/cm^2. The *upper part* shows a zone where deep surface excavation has occurred. The *lower part* shows the profile along the *horizontal line* indicated

this site. The profile along the horizontal line indicates that about 300 nm of material has been removed from the sample, while the nominal thickness of the combined silica layers is only 260 nm. This slight excess may be attributed to blistering, i.e. the formation on either side of the excavation of a raised-up zone where the gold nanoparticles have expanded without provoking a fracture in the silica layers. This profile also illustrates the extreme fragility of the sample at the interface between the polished substrate and the deposited layer. In this sample, the high density of the inclusions ($100/\mu m^2$) makes it impossible to isolate the effect produced by a single nanoparticle. The mean interparticle distance of 100 nm is comparable to the 130-nm thickness of the layers, which suggests that collective effects are probably important. Consequently, in the following sections we confine our attention to the d_{10} samples.

4 Time-of-flight mass spectrometer

The schematic drawing shown in Fig. 5 indicates the principal elements of the CHARISMA time-of-flight mass spectrometer at Argonne National Laboratory, which has been described in detail elsewhere [20–22]. One may distinguish five major components; an ion source, the main laser for target irradiation, the secondary laser for ionizing the ejected material, the vacuum chamber and the time-of-flight mass spectrometer.

The ion source provided 5-keV Ar^+ ions, which struck the target at an angle of 60° from the surface normal. The beam diameter was about 1 mm, and the current was adjusted between 0 to 1.5 µA. The main laser was a diode-pumped Nd:YAG whose frequency was tripled ($\lambda = 355$ nm). Its beam had an axially symmetric Gaussian profile in space, with a diameter on the target of 30 µm at $1/e$ intensity. The laser was pre-programmed to deliver a burst of 256 pulses of 8-ns duration (FWHM) at a repetition rate of 1 kHz. Since the laser beam struck the target at an angle of 60° from the normal, the impacted surface was an ellipse. The polarization of the

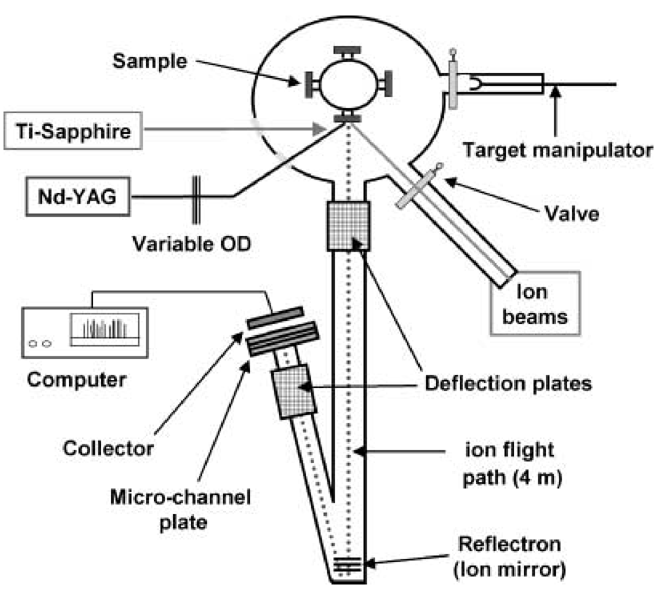

FIGURE 5 Schematic picture of the time-of-flight mass spectrometer

beam was "P", and the maximum energy of a single pulse was 370 µJ. A variable-density optical attenuator was used to manually adjust the energy of the laser between each burst of 256 shots. Theoretical [23] and experimental [24–26] work has long ago demonstrated that the damage thresholds for pulses of duration > 1 ps depend essentially on a single parameter, $F/\sqrt{\tau}$, where F denotes the fluence of the pulse, and τ its duration. The "effective" fluence corresponds to a conventional 3-ns pulse duration, which is generally used in the framework of laser-induced damage studies. The quantity F_{eff} is thus simply related to the true fluence, F_{real} by $F_{\text{eff}} = F_{\text{real}}\sqrt{\tau_{\text{eff}}/\tau_{\text{real}}}$, with $\tau_{\text{eff}} = 3$ ns. Throughout the remainder of this paper, the fluences indicated will refer only to "effective" fluences, F_{eff}, corresponding to pulses of 3-ns duration.

The 3rd harmonic of a tunable Ti:sapphire laser ($\lambda = 267.674$ nm) was used to ionize the gases emitted from the target as a result of the damage-inducing irradiation. The laser wavelength was chosen to resonantly ionize Au (via the first $2s \rightarrow 2p$ transition, followed by a second photon of the same color), however the photon energy was sufficient to effect non-resonant two-photon ionization of a variety of other species such as Si and $Si_xO_yH_z$ as well. The Ti:sapphire beam was directed parallel to the target face, and illuminated an area whose cross section was 1 mm × 3 mm. The pulse duration of this laser was 25 ns and the pulse energy was 45 µW at the target.

The main chamber could contain as many as four targets, and the vacuum in it was 10^{-9} Torr. A target manipulator operating through a lock allowed one to place the targets on a wheel which could be moved from the exterior. Each target could be translated and rotated so as to align it with the laser beams and optimize the ion yield in the mass spectrometer. The ions (generally those produced by ionization of the neutral vapor) were accelerated by a potential difference, drifted through a tube and underwent a reflection at a reflectron, where a variable electrostatic potential was used to reduce the dispersion in velocity and improve the mass resolution. The total flight path was 4 m. A micro-channel plate was used to collect the ions. The resulting signal then consisted of counts per unit time as a function of time; it was then fed to a data-acquisition system for further treatment. In the experimental set-up there was also an optical Schwarzschild microscope in the vacuum chamber (not shown in the figure), which permitted us to continually observe the irradiated zone and thus to see any damage produced by a burst of 256 shots. In order to avoid charge accumulation, the silica surface was covered by a grid of fine chromium strips, spaced 500 µm apart. The microscope also allowed us to position the target so as to avoid irradiating these strips.

This experimental system could function either by bombarding the target with argon ions or by irradiating it with the UV laser beam. We mainly used the laser beam. The ion beam was used only to calibrate the spectrometer by bombarding a thin film of gold. It was also used to check that the target surface was clean before a laser shot (detection of possible contamination by gold vapor emitted during preceding shots). In Fig. 6 we show a Nomarski microscope photograph of the principal irradiated zone of a sample. The chromium strips mentioned above are clearly visible on the photograph. In this

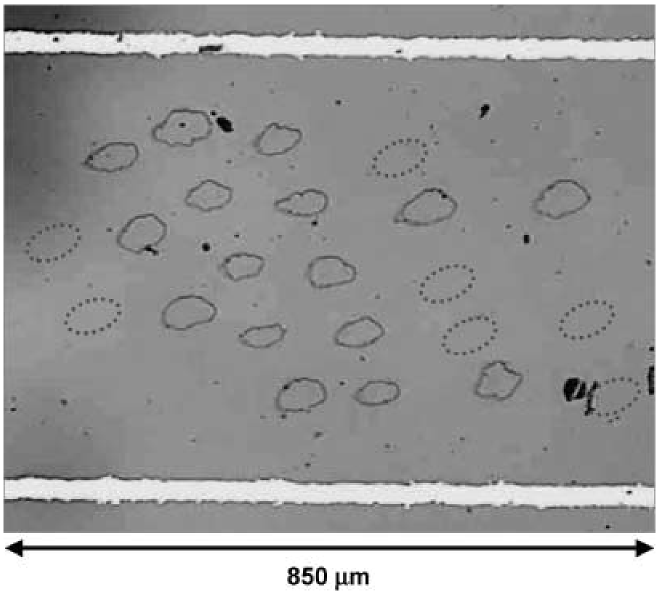

FIGURE 6 Nomarski photograph of the principal irradiated zone on a sample. Each damage site corresponds to one burst of 256 shots. Some sites, where no damage was observed, are indicated by *dashed ellipses*. The chromium strips used to evacuate any charge on the sample are clearly visible

zone, a number of 256-shot laser bursts were made. Several of the damage sites are clearly visible, while some irradiated spots, where no substantial damage may be seen, are shown as dashed ellipses.

5 Mass spectra corresponding to a burst of 256 laser shots

In Fig. 7 is displayed a typical mass spectrum for one of our prepared gold-bearing samples. This spectrum corresponds to one 256-shot laser burst at a main laser fluence of 5.5 J/cm^2. Each atomic or molecular ion which enters into the spectrometer is unambiguously identified by its time of flight. The vertical scale indicates the number of laser shots (among the 256) for which at least one ion was counted in the appropriate time interval. If, for a given ion, at least one was detected on each shot, then that ion would have an intensity of 256 in Fig. 7.

This spectrum shows a large number of different components: the alkalis (Li, Na, K), which frequently contaminate the surfaces and are easily ionized, the gold coming from the nanoparticles, and all the silicon compounds which are produced by decomposition of the silica under intense laser irradiation. We see a large number of such compounds, ranging from atomic silicon to complex oxides and hydrates of silicon containing as many as 20 atoms. Some of these contain hydrogen, which was present initially as residual water in the silica matrix. We also note the absence of any other major metallic contaminant. These mass spectra, obtained with the spectrometer functioning in this binary mode, provide a good qualitative picture, but do not represent the relative intensities of ions emitted by the target. However, it is also possible to obtain a quantitative analysis, provided the mass range is sufficiently limited. This will be discussed later.

The spectrometer detected both ions directly emitted by the laser-irradiated target as well as neutral atoms or molecules, which were subsequently ionized by the Ti:sapphire laser. A comparison of spectra taken with and without the Ti:sapphire ionizing laser showed that the ion yield without the Ti:sapphire laser was substantially less than when the laser was used. In particular, gold was not observed without the ionizing laser. Thus in all the results we show, the ionizing laser was used. We estimated approximately 0.05 to 0.1% of the vaporized gold atoms emitted by the target were detected by the spectrometer when the ionizing laser was used.

In Fig. 8 are shown six mass spectra obtained at fluences ranging from 1.9 to 6.3 J/cm^2, each corresponding to a fresh site and a 256-shot burst. On the right-hand side of

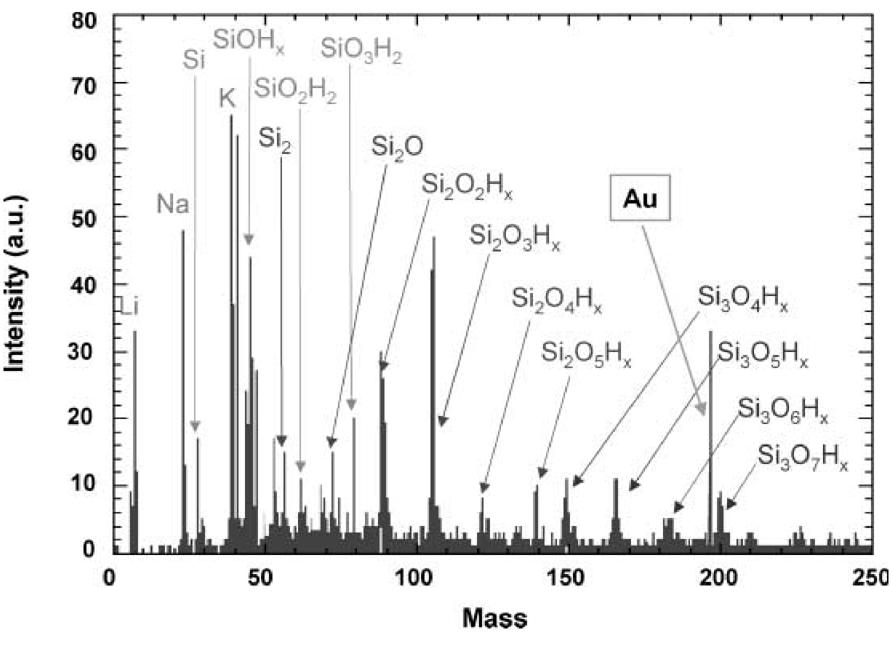

FIGURE 7 Typical mass spectrum obtained after laser irradiation by one burst of 256 shots at a fluence of 5.5 J/cm^2 on a sample containing gold nanoparticles. The principal atoms (Au, Li, Na and K) and silicon compounds are labeled in the spectrum

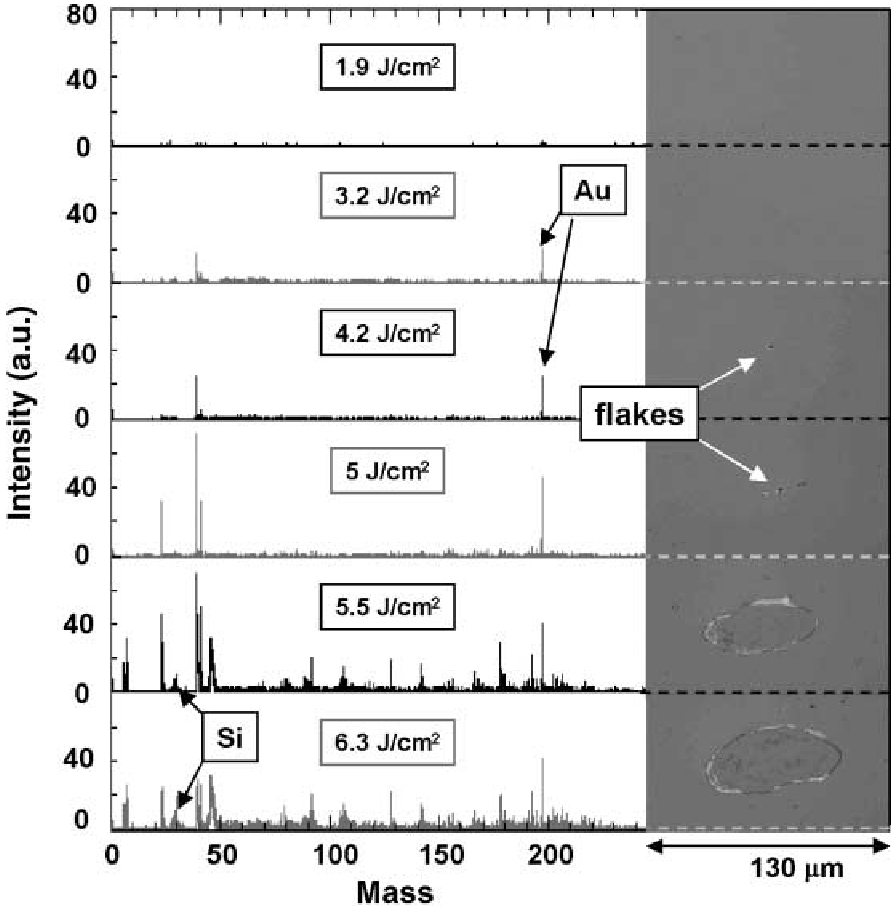

FIGURE 8 Six mass spectra (obtained at the fluences indicated) and the corresponding Nomarski microscope photographs of the damage produced by the burst of 256 shots. Each spectrum corresponds to a fresh site

the figure, Nomarski microscope photographs of the surface damage corresponding to each spectrum are indicated. We point out two interesting ranges of fluence. Between 3 and 5 J/cm^2, gold is clearly detected, but no substantial amounts of silicon-containing compounds are seen. However, beginning at 5.5 J/cm^2, silicon, as well as several of its compounds, appears in significant quantities. The Nomarski images correlate with the spectra in the sense that in the 4–5 J/cm^2 range only some flaking of the surface is observed, whereas the shots at 5.5 and 6.3 J/cm^2 correspond to sharply defined craters, indicating significant ejection of silica. We also point out that the gold yield doesn't increase greatly beyond what is obtained at 4.2 J/cm^2. Indeed, even at 3 J/cm^2, there is a significant gold signal in the spectrum, although the surface appears to be undamaged, even under highest resolution of the Nomarski microscope.

Repetition of bursts on the same sample allowed us to verify that our results were reproducible, and to demonstrate clearly the existence of a threshold for significant damage for fluences between 5 and 5.5 J/cm^2. The surface flaking seen at fluences of 4 and 5 J/cm^2, together with the gold observed at these and even lower fluences, proves the existence of what we call "internal" damage structures that are impossible to see with a microscope. Under these conditions, the term "predamage" seems appropriate to characterize our observations.

In order to complete this work, we performed AFM measurements on a site severely damaged at a fluence of 5.5 J/cm^2, and on a site where surface flaking was observed at a fluence of 5 J/cm^2. The results are depicted in Fig. 9a for the latter and Fig. 9b for the former. As before, we display a two-dimensional scan of the site, accompanied by a section along the horizontal lines visible in the scans. For the lower-fluence shot, the scan extends over only a square of side 10 μm, showing that the damaged surface is considerably less than the 30 μm by 60 μm ellipse that the laser beam illuminated. The profile shows that the silica has been ejected to a depth of about 250 nm over a length of 3 μm. In particular, the bulk substrate appears to be intact. The contrast with the site which received slightly greater fluence, Fig. 9b, is quite notable. The square has side 80 μm, and the damage site is quite compatible with the laser spot size which was visible in Fig. 8. Even more remarkable is the great depth observed in the section, which shows that the substrate has been evacuated to a depth of 3 μm, more than ten-times the depth reached in Fig. 9a. Thus we find that a 10% increase in fluence corresponds to a thousand-fold increase in the quantity of ejected material.

Although we see evidence for a sharp damage-initiation threshold, we must point out that this is, to some extent, linked to our operating procedure of 256-shot bursts. To study this problem, we twice carried out 256-shot exposures of three distinct sites, at fluences of 4.2, 5 and 5.5 J/cm^2, respectively. After having received 512 shots (in two separate bursts) the site illuminated with fluence 5 J/cm^2 showed the same level of damage (crater formation) as the site illuminated at fluence 5.5 J/cm^2 after only one burst. The site receiving 4.2 J/cm^2 did not form a crater, however. Thus, the notion of a sharp

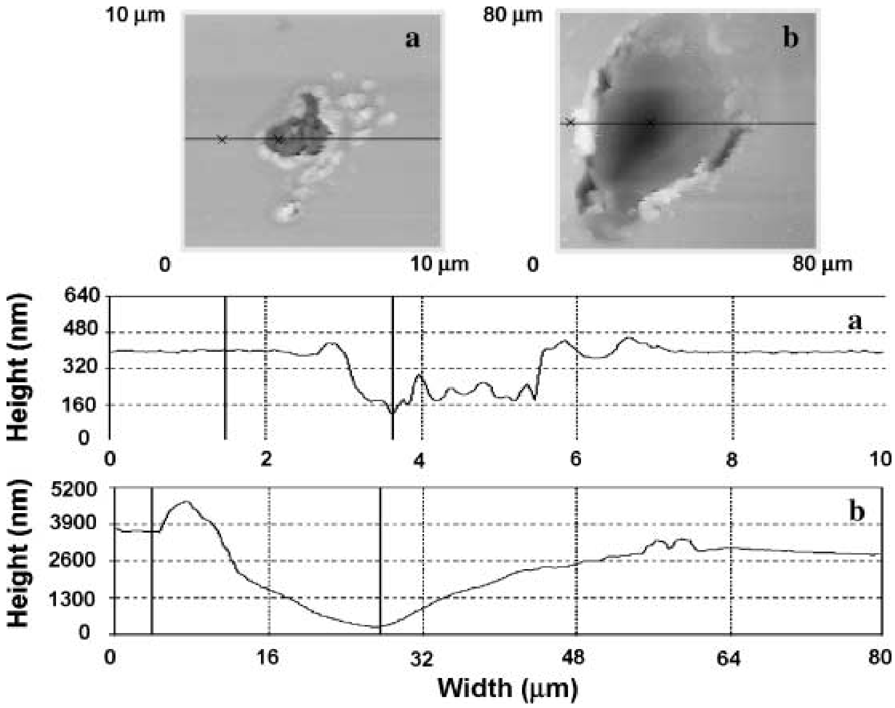

FIGURE 9 AFM observation of two sites damaged at different laser fluences; 5 J/cm^2 (**a**) and 5.5 J/cm^2 (**b**). The *upper part* shows a two-dimensional scan of the damaged zone (note different scales), while the *lower part* shows the profile along the *horizontal lines* indicated

threshold must be modified to take into account some cumulative effects in addition to the fluence. In order to get more information on this phenomenon, we modified our experimental procedure to study the shot-by-shot emission of ions, but this could only be done by limiting the mass spectrum to a very narrow interval. We discuss these results in the following section.

6 Observation of the time dependence of ion emission

The data acquisition system of the mass spectrometer could function in different modes. The previous results were obtained in a yes–no mode, in which a time interval having more than a given threshold number of counts is credited with 1, and 0 if the threshold is not reached. However, provided that only a narrow portion of the spectrum was acquired (i.e. shorter time intervals), it was possible to analyze the spectra on a shot-to-shot basis and determine the number of ions of a given mass produced by each shot. Data treatment requirements limited this mode of operation to the first 100 shots from the 256-shot burst. In Fig. 10 we show the spectra of the first three shots of a burst at a fluence of 5.5 J/cm^2. The mass region shown is limited to a narrow region around 197, the mass of a gold atom, and the excellent resolution of the system is apparent. The small dispersion in mass that is seen is

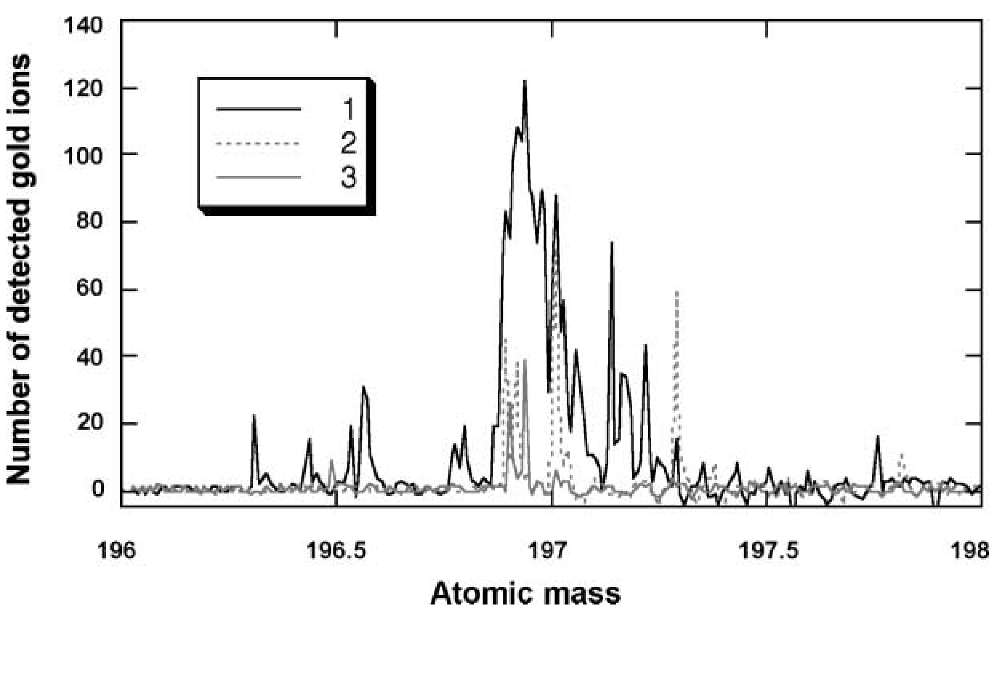

FIGURE 10 Mass spectra for the first three shots (denoted by 1, 2 and 3) of a laser burst at a fluence of 5.5 J/cm^2. Only the mass region in the neighborhood of gold is shown

due to some initial velocity dispersion of the neutral atoms, as well as to the uncertainty in the height above the surface at which any given emitted neutral atom was ionized. This figure clearly shows that the first shot liberates many more gold atoms than its two successors.

By choosing the appropriate narrow intervals, we could study the emission of silicon compounds as well as gold ions as a function of the shot number. Some of these results are shown in Fig. 11. In each case, the fluence was 5.5 J/cm^2, and a different site was used for each different ion that was analyzed. For the two ions of greatest interest to us, gold and silicon, several irradiations (on distinct sites) were made to verify the reproducibility of our results. Two of these runs were analyzed and are shown as solid and dashed curves. The main conclusion to be drawn from these observations is that the gold atoms of the sample are emitted in the early shots, in particular the first, while the major part of the silicon and its compounds appear only much later, after at least 60 shots. We thus observe a marked decoupling between the emission of gold and that of silicon and its compounds.

In view of the results displayed in Fig. 11, we propose the following mechanism to explain our observations. Firstly, the very early liberation of gold atoms implies that even at the first shot, the gold nanoparticles must reach melting or vaporizing temperatures, releasing atoms which are able to migrate 130 nm to reach the surface, where they are emitted and subsequently ionized by the Ti:sapphire laser. During this early phase (< 20 shots), much of the gold is liberated, although no notable damage to the silica matrix occurs. Next comes a long incubation phase, in which only small amounts of the remaining gold are liberated, and no measurable quantities of silicon are released. We conjecture that during this phase the remaining gold diffuses throughout the silica matrix, leading to substantial changes in its optical properties, in particular its absorption. Finally, when the optical properties are sufficiently modified, the matrix itself begins to strongly absorb UV laser light, and to suffer considerable damage, leading to the release of large amounts of silicon and its compounds, along with a relatively small amount of gold. We assume this gold is released from the slowly expanding boundary of the damage site.

We observed earlier that the threshold for severe damage decreased from 5.5 J/cm^2 to 5 J/cm^2 when we made two bursts on the same site, instead of one. In view of the interpretation given above, its seems natural that the period of incubation lasts longer for lower fluence. In order to test this, we have extended our observations to include three bursts of 256 shots on the same site, again with the small interval of the mass spectra containing the gold ions on a shot-by-shot basis. Once more we were limited to the first 100 shots of each burst by the data analysis. In order to compare the effect of the fluence, we used fluences of 1.9, 3.2, 4.2, 5 and 5.5 J/cm^2. The results are displayed in Fig. 12, along with the Nomarski microscope photographs of the corresponding sites, each having received all three bursts. Technical problems prevented the data acquisition for the third shot at fluence 3.2 J/cm^2, and only the first two are shown.

This figure contains several notable aspects. Among these we point out that the damage site photographs clearly show that the major damage threshold has decreased to 4.2 J/cm^2 with the addition of the third burst. This confirms that the threshold is not just a function of fluence, but also of the cumulative history of the sample. We also note that surface flaking has now occurred at 3.2 J/cm^2, which did not happen after

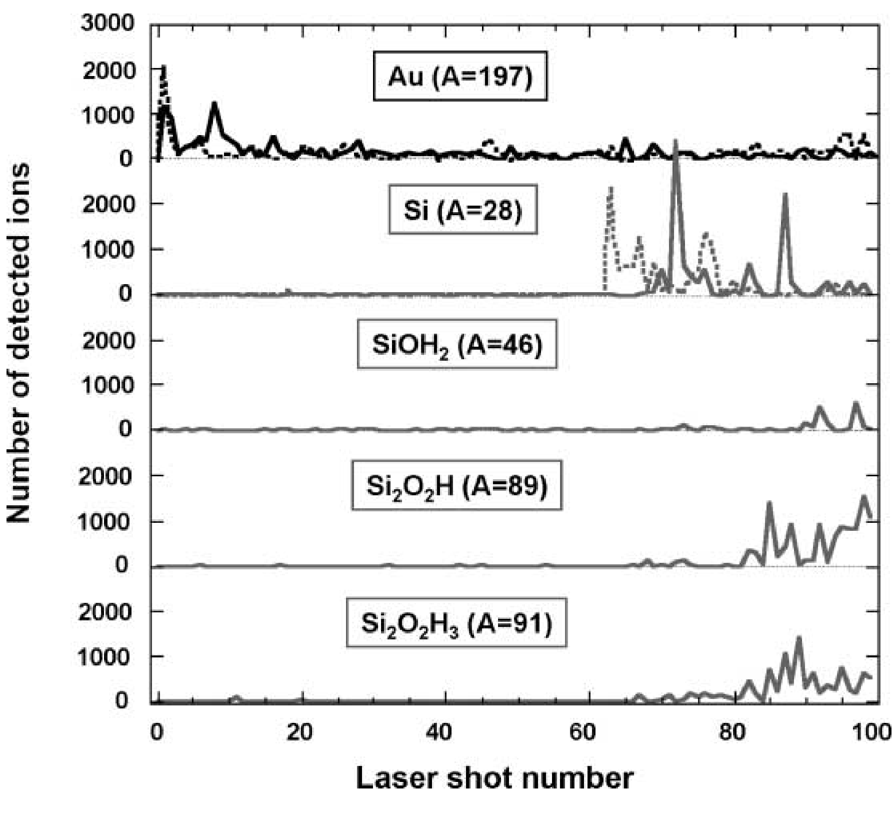

FIGURE 11 The number of gold ions and principal silicon compounds observed as a function of the shot number for laser bursts at a fluence of 5.5 J/cm^2. The *dashed* and *solid curves* for gold and silicon correspond to distinct sites, and provide an indication of the reproducibility

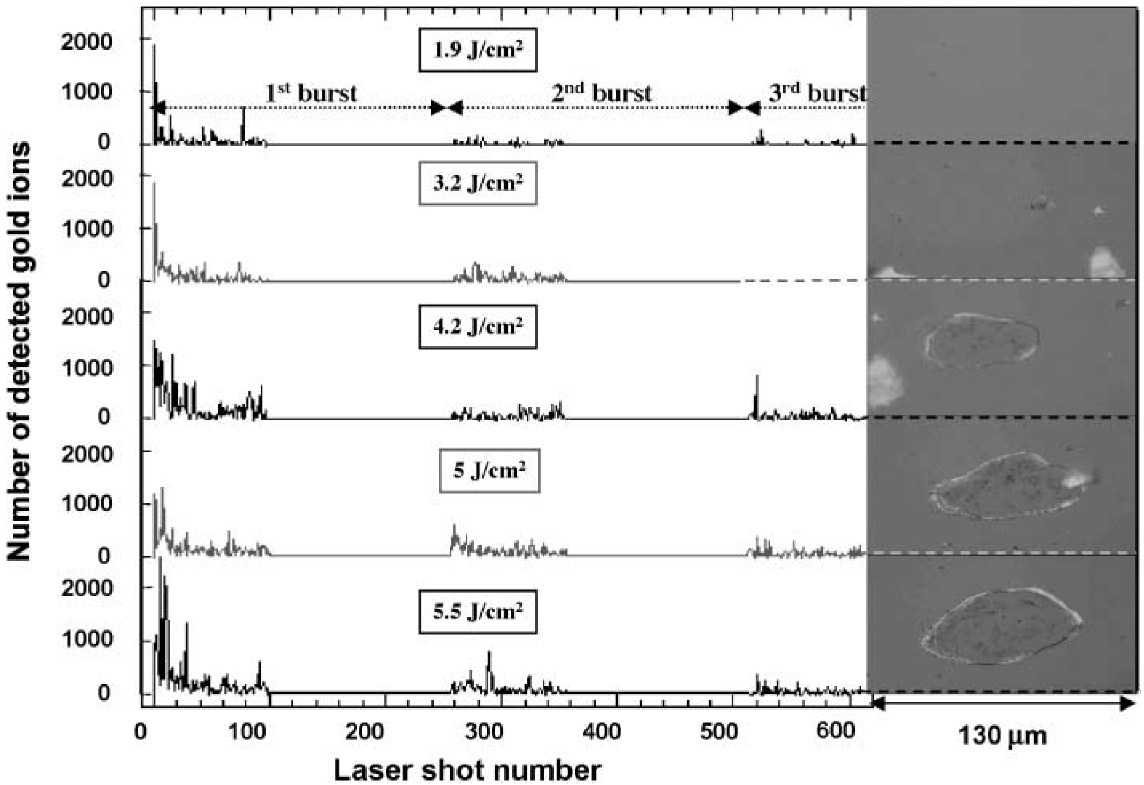

FIGURE 12 The number of gold ions detected as a function of shot number for the first 100 shots of three consecutive bursts on the same site at the fluences indicated. On the *right* are shown corresponding Nomarski microscope photographs of the damaged sites after receiving three bursts of 256 shots

one burst (Fig. 8). By extrapolating this trend, we conjecture that after a few more bursts at this fluence massive damage might be produced. However, for fluence $1.9\,\mathrm{J/cm^2}$ we still observe no damage. In contrast to these different levels of surface damage, the number of gold ions emitted as a function of shot number shows much less variation with laser fluence. Once again, it appears that most of the gold ions are emitted in the first few shots, and relatively few afterwards, even after the sample has received a great number of shots. This relative independence of the gold yield on the fluence constitutes the most puzzling aspect of these results. In order to further investigate this question, it would be necessary to conduct an experiment which permits single shots, coupled with some means of observing surface damage. We are currently designing an apparatus to do this.

7 Modeling and numerical simulations

For the modeling and simulation of laser-induced damage in glasses, we employed the code "DELPOR" developed by the CEA [27]. This is a one-dimensional Lagrangian hydrodynamics code, which has been adapted to include the laser–matter interaction. It allowed us to calculate, with the help of multi-phase equations of state [28], the evolution of matter from the solid to the plasma states under the influence of energy deposited by the laser [29]. The solution of the Helmholtz wave equation permitted us to determine the electromagnetic field throughout the region illuminated by the laser. We could then deduce, with the help of a large data bank of transport coefficients, indices of refraction [30], electrical and thermal conductivities of dense [31] or tenuous [32] plasmas etc., and the energy deposited by Joule heating. The code then determined the flow, by heat conduction and radiative transfer, of this energy throughout the irradiated target. It could also take into account ionization of the silica by electronic avalanche [33, 34], multi-photon absorption [35] or the photoelectric effect caused by the UV radiation emitted by the inclusion when it reached high temperature.

We have studied the effect of a spherical metallic inclusion placed at a given depth in a silica substrate. To describe the interaction of the absorbing inclusion with the laser, which we assume to be a normally incident monochromatic plane-wave propagating in the vacuum, we used Mie's theory [36, 37] to obtain an exact solution of the Helmholtz equation. The code DELPOR incorporated the Mie solution and extended it to include a radial gradient of the index of refraction. The electromagnetic field calculated with the help of this theory presents either a two-dimensional structure (for circularly polarized incident light), or a three-dimensional structure (for linear polarization). As an illustration of the model, we show in Fig. 13 a contour map of the modulus of the electric field in the plane of polarization. The inclusion in the silica is a gold sphere of diameter 3 nm, irradiated by a laser of wavelength $\lambda = 351$ nm. We point out that in the silica, the electric field at the poles of the inclusion exceeded the unperturbed incident field by a factor of 2.55.

Mie theory allowed us to evaluate precisely the amount of energy absorbed by a solid cold metal sphere inserted in silica, as a function of its initial size. Figure 14 shows, for two different wavelengths, and as a function of the radius, the ratio of the energy absorbed by the sphere to the unperturbed energy traversing a disk of the same radius. This ratio is very

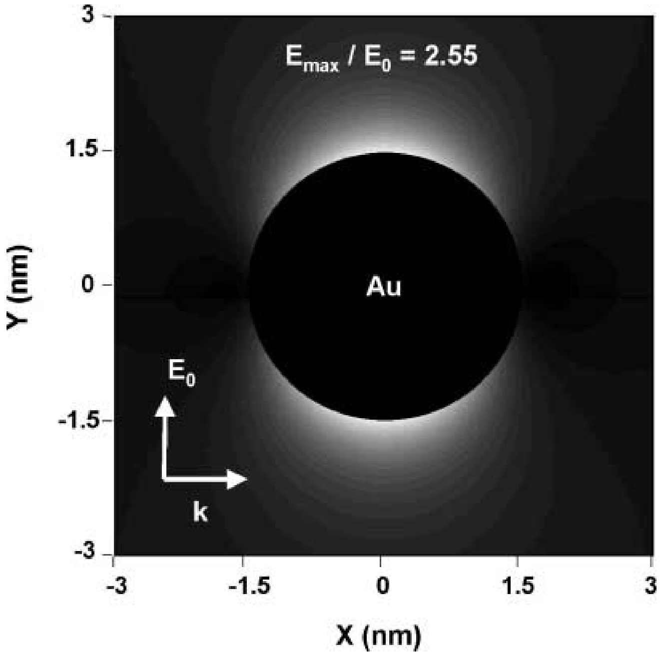

FIGURE 13 Map showing contours of constant modulus of the electric field generated by a plane wave ($\lambda = 0.351\ \mu$m, linear polarization) around a gold sphere of 3 nm surrounded by silica. The *plane* shown is spanned by the directions of propagation and polarization of the incident laser beam

sensitive to both the wavelength of the radiation and the size of the inclusion. Very small particles absorb only a small fraction of the energy they "see". For the inclusion contained in our samples (diameter = 3 nm), this fraction was 10% at 3ω, and 5×10^{-4} at ω. It is important to note that the absorption of the inclusion varies once its temperature begins to rise. This variation of the absorption during the irradiation was taken into account by the code DELPOR [38]. The curves shown in Fig. 14 do not include this effect, and thus are valid only at the initial instant, or for very small laser fluences.

The following results concern the interaction of a single Gaussian laser pulse of FWHM 3 ns with a spherical gold inclusion of diameter 3 nm isolated in a silica matrix (no collective effects among inclusions). For this reason, the simulations are not intended to reproduce the damage effects observed with our experimental samples. However, the thermodynamic behavior of the inclusion in the matrix as a function of laser fluence may be compared with the mass spectrometry results, in particular for the first laser shot.

We have carried out a detailed simulation of the interaction in which the influences of the coupling of the inclusion and silica, and the thermodynamic state of the inclusion, were studied parametrically. In fact, perfect thermal coupling between the inclusion and the silica is probably not a realistic assumption. Indeed, we know that the silica in these thin films is quite porous, with a density only 70% of that of bulk silica. Furthermore, it seems reasonable that even the physical contact (at the interface between the two layers of silica and with the nanoparticles) is not perfect (presence of micro-cracks and micro-cavities) [39]. In order to see the associated effects, we have varied the thermal conductivity of silica κ, from 10% to 100% of its value at ambient temperature κ_0 (at 300 K) in our simulation. The results are shown in Fig. 15. When the temperature is close to 5000 K, the absorption increases strongly and the temperature subsequently rises to a maximum value around 9000 K. This sharp increase in the absorption leads to the vaporization of gold. Then, the tenuous gold vapor no longer absorbs, and the temperature stabilizes. As was already shown for aluminum [38], the more the laser fluence is increased, the less time it takes to vaporize the inclusion without influencing the maximum value of the temperature. However, it must be noted that the temperature of the vaporized gold is not extremely high, which is consistent with the experimental result that the gold is not ionized without the Ti:sapphire laser.

As we have seen in the experimental part of this paper, gold is detected on the first laser shot for any fluence $\geq 1.9\ \mathrm{J/cm^2}$. Provided we choose a reduced thermal coupling of $\leq 20\%$ ($\kappa/\kappa_0 \leq 0.2$), Fig. 15 shows that gold is easily brought to melting point with a fluence of $2\ \mathrm{J/cm^2}$. Moreover, it appears difficult to reach vaporization if the flu-

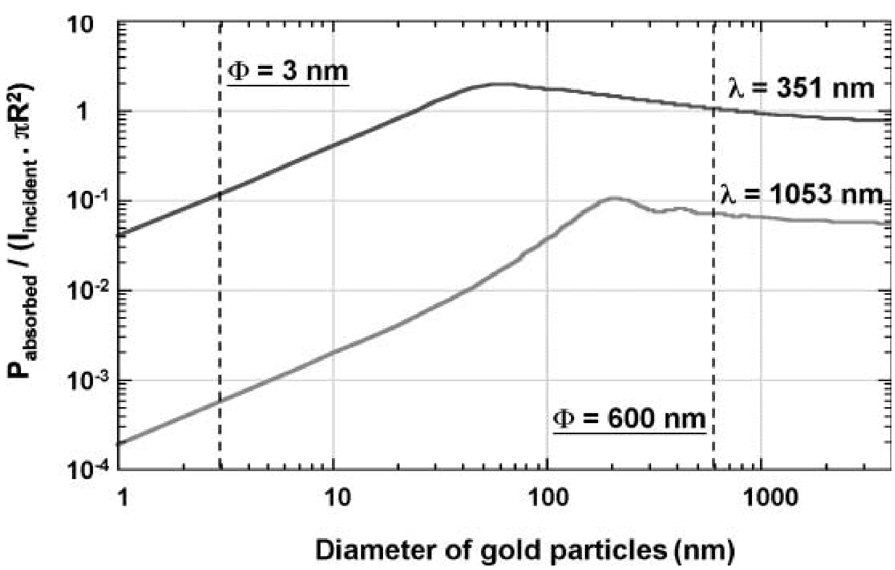

FIGURE 14 Ratio of the power absorbed by the gold sphere to that traversing a disk of identical radius, as a function of diameter, for two different wavelengths

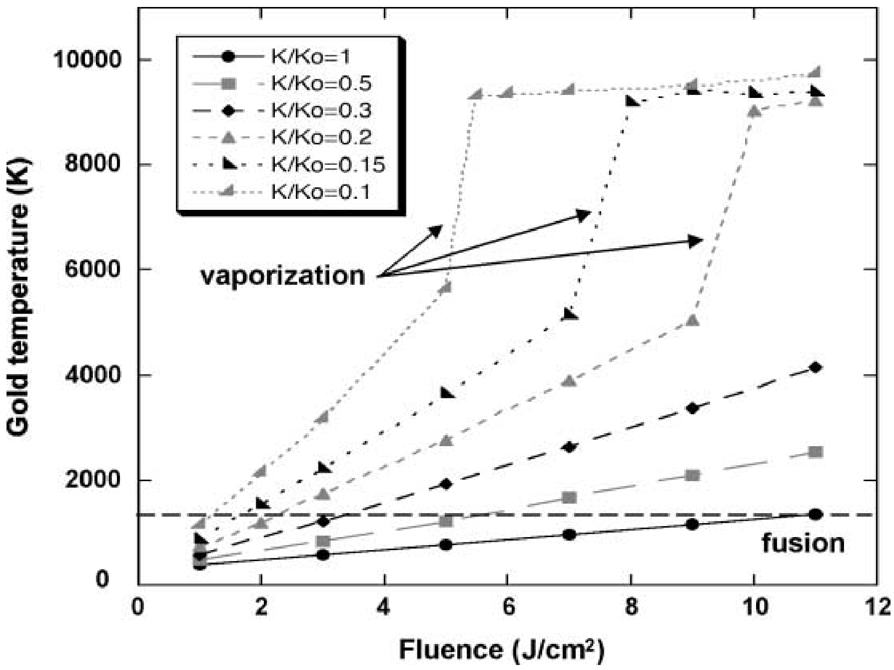

FIGURE 15 Maximum temperature reached in the gold inclusion as a function of laser fluence, assuming different values for the thermal conductivity of the silica. The melting temperature of gold is shown as a *dashed line*

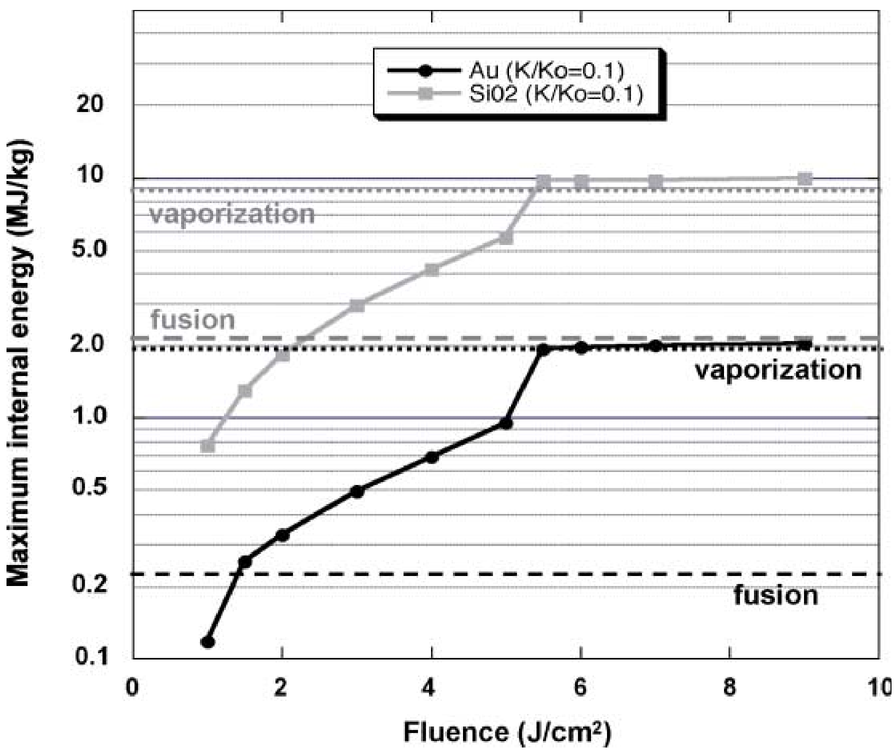

FIGURE 16 Maximum internal energy density of both gold and silica as a function of laser fluence, assuming the thermal conductivity is 10% of its value at 300 K. The melting and vaporization temperatures of gold and of silica are shown as *dashed lines*

ence is less than 5 J/cm^2, even with a coupling of 10% ($\kappa/\kappa_0 = 0.1$), and still higher fluence would be necessary if the coupling were increased slightly. If the coupling were $\geq 30\%$, no vaporization would be expected even at fluence of 11 J/cm^2. We thus conclude that vaporization is not a probable cause of the ejection of gold, and that ionization of the gold is highly unlikely. This is consistent with the experimental result that the gold is not ionized without the Ti:sapphire laser.

We recall that although gold appeared at the first laser shot, no ions of the form Si_xO_y were observed. We interpret this to mean that the silica surrounding the inclusion was not ionized. We have attempted to check this by using our most extreme hypothesis for the conductivity, $\kappa/\kappa_0 = 0.1$. With this value, we calculated the maximum temperature and internal energy in the silica. Figure 16 displays the internal energy densities of the gold and silica as a function of laser fluence. At this low value of conductivity, at a fluence of about 5.5 J/cm^2, both gold and silica are predicted to vaporize. This simulation indicates that the thermodynamic state of the Si_xO_y is in contradiction with the "experimental" hypothesis formulated above if we suppose that the vaporization of the inclusion is necessary for the detection of gold. Whereas on Fig. 16 we observe that gold starts to melt at 1.5 J/cm^2, silica melts when the fluence reaches 2 J/cm^2. If these simulations confirm that the silica is not vaporized (much less ionized) by the first laser shot under experimental conditions, it appears that only at the highest fluence is gold vaporized, and the mechanism for ejecting gold must involve gold liquid, but not gold vapor. In current simulations, when the gold that had been confined by the silica matrix reaches the melting point, a shock wave is created. Gold pressure levels as high as 2.5 GPa are reached easily at a fluence of 2 J/cm^2. This suggests that the gold detected by the spectrometer on the first shot has worked its way through fractures of nanometric size. Clearly, more experimental and theoretical work is needed to show that liquid gold is able to escape from the matrix without being accompanied by appreciable amounts of silicon compounds.

8 Conclusion and perspectives

From among the results presented in this work, we comment here on those we consider most significant:

1. Damage thresholds and gold ejection. For a given irradiated site, the combined observation of mass spectra and microscopic surface analysis shows that at a fluence of 5.5 J/cm^2 there is a clear correlation between the detection of compounds containing silicon and severe damage to the silica surface after a burst of 256 shots. However, for fluences in the range 4–5 J/cm^2, only gold was detected, and the surface damage was much less severe. Finally, no surface damage was visible under the microscope for fluences in the range 3–4 J/cm^2, although gold continued to be detected. Nevertheless, when two bursts (each of 256 shots) were made on the same site, the threshold for heavy damage decreased to 5 J/cm^2. This fluence, while not causing massive damage at once, produces the phenomenon of "aging" in the material, which finally becomes heavily damaged.
2. Ejection of gold before significant silica compounds. The time-dependent analysis of the number of ions detected in a narrow spectral range during the first 100 shots of a laser burst at 5.5 J/cm^2 has indicated a notable temporal decoupling between the emission of gold and that of silicon and its compounds. It is as if the first 60 laser shots constituted a sort of incubation period during which the gold was heated and melted, and then fractured the silica, some of it permeating throughout the surrounding silica. We conjecture that this addition of gold to the transformed silica changes its optical properties, thereby increasing its absorption. We have reached the borderline between two distinct phenomena. On one side there is heavy damage, observable by classical means and in which the silica absorbs light strongly. The other is a sort of pre-damaged state, much harder to observe, in which the ejection of gold is clearly detected, but where little or no apparent surface damage has occurred.
3. Comparison with numerical simulations. The numerical simulations carried out with the DELPOR code permitted us to evaluate, for the first laser shot, the temporal behavior of the absorption of radiation by the gold nanoparticle confined in the silica, its heating, its hydrodynamic explosion and the energy transfer to the silica by heat conduction. These simulations suggest strongly that the thermal conductivity of the silica must not exceed 10 or 20% of its ambient temperature value for bulk silica. This deduction may be justified by the high porosity of the thin films of silica (30%) and probably by poor physical contact between the inclusion and the matrix. The simulations indicate that the first laser shot does not vaporize gold but melts both gold and silica at a fluence of 2 J/cm^2. To have an interpretation in agreement with the experimental results, the mechanism for ejecting gold should involve gold liquid, but not gold vapor.

Further experimental work, particularly with samples having a lower density of inclusions, would clearly be of great interest in resolving some of the questions raised by the present paper. For example, it would be useful to irradiate such samples at the ANL mass spectrometer using a laser with variable repetition rate, including single-shot capacity. In addition, high-resolution imaging and associated analyses (FIB, SEM, EDS) or photothermal tools for accurate absorption measurements, could provide information on the damage precursors.

ACKNOWLEDGEMENTS The authors are grateful to A.V. Hamza and M.J. Fluss (LLNL) for participating at the elaboration of this study. The authors would also like to thank A. Perez (DPM) and F. Vallée (CPMOH) for fruitful discussions and encouraging this project.

REFERENCES

1 N. Bloembergen: Appl. Opt. **12**, 661 (1973)
2 B. Stuart, M. Feit, S. Herman, A. Rubenchik, B. Shore, M. Perry: Phys. Rev. B **53**, 1749 (1996)
3 A. Manenkov, A. Prokhorov: Sov. Phys. Uspeki **29**, 104 (1986)
4 P.P. Hel, D.F. Edwards: Appl. Opt. **26**, 4677 (1987)
5 K.H. Fielder: *The Properties of Optical Glass* (Springer, Berlin, Heidelberg 1995) p. 247
6 F. Genin, A. Salleo, T. Pistor, L. Chase: J. Opt. Soc. Am. A **18**, 2607 (2001)
7 J.Y. Natoli, L. Gallais, H. Akhouayri, C. Amra: Appl. Opt. **41**, 3151 (2002)
8 H. Hopper, D. Uhlmann: J. Appl. Phys. **73**, 4023 (1970)
9 M. Sparks, D. Mills, R. Warren, T. Holstein, A. Maradudin, L. Sham, E. Loh, D. King: Phys. Rev. B **24**, 3519 (1981)
10 D. Arnold, E. Cartier: Phys. Rev. B **46**, 15 102 (1996)
11 Documentation available on request from Schott Glass or Heraeus
12 S. Papernov, A.W. Schmid, R. Krishnan, L. Tsybeskov: SPIE **4347**, 146 (2001)
13 A.V. Hamza, A. Rubenchik, M. Feit, M. Savina, M. Pellin, M. Fluss, M. Nostrand, M. Runkel, M. Staggs, W. Siekhaus, I. Hutcheon: SPIE **4679**, 96 (2002)
14 S. Papernov, A.W. Schmid: SPIE **2966**, 283 (1997)
15 J. Dijon, T. Poiroux, C. Desrumaux: SPIE **2966**, 315 (1997)
16 A. Perez, P. Melinon, V. Dupuis, P. Jensen, B. Prével, J. Tuaillon, L. Bardotti, C. Martet, M. Treilleux, M. Broyer, M. Pellarin, J.L. Vaille, B. Palpant, J. Lerme: J. Phys. D **30**, 709 (1997)
17 B. Palpant, B. Prével, J. Lermé, E. Cottancin, M. Pellarin, M. Treilleux, A. Perez, J.L. Vaille, M. Broyer: Phys. Rev. B **57**, 1963 (1998)
18 J.Y. Natoli, P. Volto, M. Pommies, G. Albrand, C. Amra: SPIE **3244**, 76 (1998)
19 F. Bonneau, P. Combis, J.L. Rullier, J. Vierne, H. Ward, H. Bercegol, L. Lamaignère, M. Loiseau, M. Broyer, E. Cottancin, J. Tuaillon, M. Pellarin, L. Gallais, J.Y. Natoli, M. Perra, M. Pellin, M. Savina, M. Fluss, A. Hamza: Rapport CEA-R-6008, Saclay 2002
20 Z. Ma, R.N. Thompson, K.R. Lykke, M.J. Pellin, A.M. Davis: Rev. Sci. Instrum. **66**, 3168 (1995)

21 G.K. Nicolussi, M. Pellin, W. Calaway, R. Lewis, A. Davis, S. Amari, R. Clayton: Anal. Chem. **69**, 1140 (1997)
22 M.R. Savina, A. Davis, C. Tripa, M. Pellin, R. Clayton, R. Lewis, S. Amari, R. Gallino, M. Lugaro: Geochim. Cosmochim. Acta (2002) submitted
23 R.M. Wood: *Laser Damage in Optical Materials* (Hilger, Boston 1986)
24 D. Du, X. Liu, G. Korn, J. Squier, G. Morou: Appl. Phys. Lett. **51**, 415 (1982)
25 J.H. Campbell, F. Rainer, M. Kozlowski, C. Wolfe, I. Thomas, F. Milanovitch: SPIE **1441**, 444 (1990)
26 B. Stuart, M. Feit, S. Herman, B. Shore, M. Perry: J. Opt. Soc. Am. B **13**, 459 (1996)
27 F. Bonneau, P. Combis, J.B. Gaudry, G. Daval: SPIE **4347**, 560 (2001)
28 A.V. Bushman, I.V. Lomonosov, V.E. Fortov: Sov. Tech. Rev. B **5**, 1 (1993)
29 P. Combis, F. Bonneau, G. Daval, L. Lamaignère: SPIE **3902**, 317 (2000)
30 E. Palik: *Handbook of Optical Constants of Solids* (Academic Press, London 1985)
31 W. Ebeling, A. Förster, V. Fortov, V. Griaznov, A. Polishchuk: *Thermophysical Properties of Hot Dense Plasmas* (Teubner, Stuttgart 1991)
32 A. Decoster, P. Markowich, B. Perthame: *Modeling of Collisions* (Gauthier-Villars, Paris 1998)
33 D. Arnold, E. Cartier: Phys. Rev. B **46**, 15 102 (1992)
34 F. Bonneau, B. Cazalis: SPIE **2714**, 650 (1996)
35 L.V. Keldysh: Sov. Phys. JETPU **20**, 1307 (1965)
36 G. Mie: Ann. Physik (4) **25**, 377 (1908)
37 M. Born, E. Wolf: *Principles of Optics* (Pergamon Press, Oxford 1980) Chap. 13
38 F. Bonneau, P. Combis, J. Vierne, G. Daval: SPIE **4347**, 308 (2001)
39 H. Bach, N. Neuroth: *Analysis of the Composition and Structure of Glass and Glass Ceramics* (Springer, Berlin, Heidelberg 1998)